Raman spectroscopic studies on the ferroelectric soft mode in SnxSr1-xTi03

doi: 10.1080/00150193.2018.1430427

Raman spectroscopic studies on the ferroelectric soft mode in $Sn_xSr_{1-x}TiO_3$

Tsuguhito Nakano[1], Yu Mikami[2], Minoru Kobayashi[2], Yukihiro Kogai[2], and Kohji Abe[2]

[1]Department of Dentistry, Health Science University of Hokkaido, 1757 Tobetsu-Cho, Ishikari-Gun, Hokkaido, 061-0293 Japan.
[2] Department of Engineering Sciences, The University of Electro-Communications, 1-5-1 Chofugaoka, Chofu-shi, Tokyo, 182-8585 Japan.

tnakano@hoku-iryo-u.ac.jp

ABSTRACT

The Raman spectra of novel ferroelectric ceramics $Sn_xSr_{1-x}TiO_3$ (x = 0.1, 0.05 and 0.02) were obtained to clarify the mechanism of their ferroelectric phase transitions. Two transverse-optic modes in the ferroelectric phase showed softening toward the ferroelectric transition temperature. A comparison of the spectra obtained for $Sn_xSr_{1-x}TiO_3$ with the spectrum of $Pb_xSr_{1-x}TiO_3$ facilitated the assignment of the observed modes under the assumption of the ferroelectric phase in C_{4v}^1 symmetry. However, several peaks violating the Raman selection rules were observed, suggesting the emergence and growth of polar regions even in the paraelectric phase.

Keywords: Ferroelectricity; Raman scattering; $Sn_xSr_{1-x}TiO_3$

1. Introduction

Substitution of the A and B sites of $SrTiO_3$ (STO) with various elements can induce ferroelectricity and/or change the structural phase-transition temperature. As a result, the tuning of the transition temperature and dielectric properties through appropriate substitutions has been the subject of many previous investigations. [1, 2]

Since STO is a quantum paraelectric crystal, its dielectric permittivity saturates at very high values below ~4 K owing to quantum fluctuations. Under these conditions, ferroelectric transition is suppressed. Quantum paraelectricity easily becomes unstable under the effect of external perturbations, as illustrated by the following example: if 0.2% of Sr is replaced with Ca, quantum ferroelectricity is exhibited. [3, 4] Furthermore, when Ba or Pb is substituted for Sr, the crystal structure approaches that

of $BaTiO_3$ or $PbTiO_3$, respectively, and these materials become ferroelectrics. [1, 2] Isotopic effects are also important. The substitution of oxygen with its heavier isotope O^{18} suppresses quantum fluctuations and induces ferroelectric behavior. [5]

In 2012, Suzuki et al. reported on the ferroelectricity of $Sn_xSr_{1-x}TiO_3$ ceramics (hereafter denoted as SSTO), which are obtained by substituting Sr with Sn in STO.[6] Their work was motivated by a first principles study of pure $SnTiO_3$. This study suggested that the spontaneous polarization of $SnTiO_3$ is larger than that of $PbTiO_3$ (PTO). [7] The temperature dependence of the dielectric permittivity (ε') of SSTO is described by a broad peak, such that the peak temperature T_m gradually increases with the concentration of Sn. For SSTO with the highest replacement rate $x = 0.1$, T_m increases to ~180 K. Although this broad peak is characteristic of a relaxor, the frequency dependence of ε' weakens as the concentration of Sn increases. Below T_m, a weak *D*-*E* loop is observed. [6] Since SSTO has a high dielectric permittivity and broad peak near room temperature owing to the shift of T_m due to Sn substitution, it has attracted significant attention as a new lead-free dielectric material.

Several experiments also were performed by Suzuki et. al, in order to investigate the mechanism of ferroelectric transition. [6, 8] X-ray diffraction (XRD) results for SSTO $x = 0.1$ obtained using a laboratory diffractometer suggest that the lattice constants change at T_m due to a structural change from a cubic to tetragonal system. [6] The measured values of pyroelectricity show that polarization gradually increases upon cooling from room temperature to T_m. [6] Spherical-aberration-corrected scanning transmission electron microscopy (Cs-STEM) together with energy-dispersive X-ray spectrometry (EDX) has revealed Sn atoms located at off-centre positions in some lattice sites even at room temperature. [6] Moreover, using piezoresponse force microscopy (PFM), microscale-polar regions distributed inhomogeneously at room temperature have been detected. [8]

In 2014, the authors reported the tentative assignment of the Raman spectra of SSTO ceramics. [9] As the structural change in SSTO was not decided at that time, we assumed that the freezing of R_{25} mode accompanied by the change of symmetry from O_h into D_{4h} causes the observed structural phase transition. However, synchrotron-radiation XRD and x-ray absorption fine structure (XAFS), [10] and neutron diffraction [11] analyses have shown that the structural change at T_m is associated with the displacement of the B site atom and the octahedral oxygen in the opposite direction along the c-axis. This is similar to the ferroelectric transition of PTO in that the space group changes from $Pm\bar{3}m$ (O_h^1)

to $P4mm$ (C_{4v}^{1}). This is also consistent with the displacement predicted by the first-principles calculations performed for $SnTiO_3$. [7] These studies also show that the local distorted structures around Sn atoms exist in the paraelectric phase. [10, 11]

Since these results contradict the model that was originally proposed by the authors, [9] the Raman spectra of ferroelectric $Sn_xSr_{1-x}TiO_3$ were measured again in the present study in order to fully determine mode assignments. In Ref [9], two soft transverse optic modes were assigned as A_{1g} and E_g in D_{4h}^{18} which are related to the structural soft mode R_{25}. In this paper, it was found that those two modes are associated with the F_{1u}(TO1) ferroelectric soft mode at Γ-point. The assignments of other modes were reconsidered based on the spectra of $PbTiO_3$ and $Pb_xSr_{1-x}TiO_3$. [12, 13] Spectra were recorded at temperature higher than the room temperature for SSTO $x = 0.1$ in order to investigate the origin of the pyroelectricity in the paraelectric phase.

2. EXPERIMENTAL PROCEDURES

Ceramic samples of $Sn_xSr_{1-x}TiO_x$ ($x = 0.1$, 0.05, and 0.02) and $Pb_{0.15}Sr_{0.85}TiO_3$ (PSTO $x = 0.15$) were prepared by Suzuki at Murata Manufacturing Co. Ltd. [6,14] The samples had a typical size of 3 × 3 × 1 mm^3 and an average grain size of approximately 200–500 nm. They were cooled in a helium flow-type cryostat. The micro-Raman technique was employed using a long-working-distance objective lens (BD Plan Apo10 ×, Mitsutoyo, NA = 0.28, WD = 33 mm). An Ar^+ laser (wavelength = 514.5 nm) was used as the excitation light source, and backscattered light was collected by the objective lens without a polarizer. The laser power was carefully adjusted in order to prevent local heating of the sample. To obtain spectra over the frequency range of 200–700 cm^{-1}, a single spectrometer (Spectra Pro275, Acton Research with a resolution equal to 4.0 cm^{-1}) with an intensified CCD (ICCD-1152MG-E, Princeton Instruments) was used. For the very-low-frequency region 5–80 cm^{-1}, a double monochromator (U1000, Jobin-Yvon) was employed. The spectral resolution was set to 1.8 cm^{-1}. To measure the SSTO $x = 0.1$ spectra over the temperature range of 120–500 K, the sample was set to a temperature-controlled stage. Scattered light was analyzed using a spectrometer (NR-1800, JASCO, resolution = 1.4 cm^{-1}) with an ultralong-working-distance objective lens (ULWD CDPlan40, Olympus, NA = 0.5, WD = 13 mm). When the temperature was raised above room temperature, the sample room was purged with nitrogen to prevent deterioration of the sample surface.

3. RESULTS AND DISCUSSION

3.1 *Spectra of SSTO in very-low-frequency region*

Figure 1(a) shows the temperature dependence of the Raman spectra of SSTO with x = 0.02, 0.05, and 0.1 in the frequency range of 5–80 cm^{-1}. To clearly determine the behavior of these modes, the reduced Raman spectra $\mathrm{Im}\chi(\omega) = I(\omega)[1 + n(\omega)]^{-1}$are shown in Figure 1(b), where $I(\omega)$ is the Raman intensity and $n(\omega)$ is the Bose factor. For x = 0.1, three Raman peaks, two peaks are observed at ~26 and ~44 cm^{-1} with a further large peak at ~77 cm^{-1}, are observed at 20 K. The latter peak illustrates the softening with a decrease in temperature and overlaps with the former two peaks for low Sn concentrations. For all values of Sn concentration, the following behavior is observed: as the temperature decreases from 300 K, the area intensity of the spectrum in the low-frequency range increases and two peaks appear near T_m. (The values of T_m for SSTO x = 0.1, 0.05, and 0.02 are 180, 150 and 90 K, respectively). Below T_m, the frequencies of these peak increase to ~26 and ~44 cm^{-1}. Since the temperatures at which these peaks appear are in agreement with the T_m for the corresponding Sn concentration, these two modes are considered as the ferroelectric soft modes.

However, owing to the strong intensity of Rayleigh scattering and the strong anharmonicity of the soft modes, it is difficult to determine whether the soft mode freezes or not. At temperatures higher than T_m, it seems that the intensity of the overdamped mode increases toward T_m. We assumed that this behavior is indicative of the relaxation mode. Further analysis of the low-frequency region using other models will be performed in future work by taking into account the coupling of soft modes and the effects of the ferroelectric microregion (FMR). [15]

3.2 *SSTO x=0.1 and PSTO x=0.15 in wide spectral range*

Figure 2(a) shows the Raman spectra of SSTO x = 0.1 in the frequency range of 15–700 cm^{-1}. At $T = 300$ K, broad peaks at ~120 and ~545 cm^{-1} and an asymmetric peak at ~173 cm^{-1} are observed. In addition to these modes, a broad peak at ~120 cm^{-1} ($T = 300$ K) splits into two peaks at $T \sim T_m$ upon cooling. Of these peaks, the lower-frequency component decreases to 77 cm^{-1}. Below T_m, the peaks at ~267 and ~444 cm^{-1} become clearer. Two modes that appear below 50 cm^{-1} are the ferroelectric soft modes, as was shown in Figure 1.

For comparison with SSTO, Raman spectra of displacive-type ferroelectrics $Pb_{0.15}Sr_{0.85}TiO_3$ (PSTO $x = 0.15$) are shown in Figure 2(b). PSTO x=0.15 undergoes the ferroelectric transition at T_c=170 K with the symmetry changes from $Pm\bar{3}m$ (O_h^1) to $P4mm$ (C_{4v}^1). [1,2] This symmetry change is the same as that observed in SSTO with the neutron scattering. [11] The overall spectral structure of PSTO x = 0.15 is very similar to that of SSTO, except that no peaks appear above T_c and their line widths are relatively narrow.

3.3 *Mode Assignment*

The mode assignment of the PSTO x=0.15 spectra in Figure 2(b) was obtained with reference to the Raman-scattering studies on PTO single crystal [12] and PSTO x=0.2 and 0.3 ceramics. [13] In ref. [13], the large splitting of E-mode with lowest frequencies was attributed to the symmetry breaking by the A-site cation. [16, 17] However, since it is not clear whether the effect of A-site cation is same in the case of Sn substitution as the Pb case, for the assignment of the spectra below ~100 cm^{-1}, we referred to the PTO single crystal spectra in ref. [12].

In the paraelectric phase, no peaks are observed as expected from Raman selection rules. Below T_c (170K), several peaks are observed owing to the reduction in symmetry. A couple of peaks at ~ 27 and ~50 cm^{-1} at 20 K (shown by the arrows in the inset of Figure 2(b)) are assigned as the ferroelectric soft mode E and A_1 mode in C_{4v}^1 originate from F_{1u}(TO1) in O_h^1. [12] Then, two peaks split at about 80 cm^{-1} and 120 cm^{-1} which are from the single peak at ~ 95 cm^{-1} are the corresponding LO modes, namely E(LO1) and A_1 (LO1) . [12] LO components are observable in the backscatter geometry because the sample is ceramic. [13] A tiny peak at ~470 cm^{-1}, which is clearly seen in the spectra of PSTO $x \geq 0.2$, is also an LO component, namely A_1+E from F_{1u}(LO2). [13]

From the comparison with the spectrum of PSTO allows the peaks at approximately 26, 44, 77 and 120 cm^{-1} in the spectra of SSTO are assigned to be E (TO1), A_1 (TO1), E (LO1), and A_1 (LO1) in C_{4v}^1, respectively. They originate from F_{1u}(TO1) and F_{1u}(LO1) in O_h symmetry. The remaining peaks in the spectra of SSTO were assigned in the similar way and the results are summarized in Table 1.

We note that in contrast to the PSTO spectrum, the peaks at ~ 120 cm^{-1} (LO1), ~173 cm^{-1} (TO2) and ~555 cm^{-1} (TO4) are found in the paraelectric phase in the SSTO spectra. In ABO_3 cubic perovskite compounds, four triply degenerate optical modes $3F_{1u} + F_{2u}$ are Raman-forbidden. Therefore, these

peaks violate the Raman selection rules. The appearance of these peaks is considered due to the existence of local polarizations. Such effects are found also in the Raman spectra of STO ceramics, films, and nanocubes. [18-20] Moreover, since the grain sizes of the PSTO and SSTO samples are approximately the same, Sn doping may be the reason for the breaking of the local centrosymmetry. This is consistent with studies that reported Sn atoms located at off-centered positions using Cs-STEM [6].

3.4 *Sn-concentration dependence*

Raman spectra of SSTO for x = 0.05 and x = 0.02 are shown in Figure 3. Although no great differences are observed between the spectral features and temperature dependence among the three samples, we note that the relative intensity of TO4 at 545 cm^{-1} to the background ~620 cm^{-1} in the paraelectric phase is much weaker for x=0.02 than x=0.1. This result would be related to the existence of local polarization caused by Sn doping since the symmetry changes in SSTO x = 0.05 and 0.02 would be the same as that observed in SSTO x = 0.1. However, the reason for the lack of peak at ~444 cm^{-1} only for x=0.05 is unknown and requires further investigation.

Since PSTO x~0.025 retains the structural phase transition due to the condensation of the R_{25} mode at ~90 K as was shown in ref. [1, 2], the effect of Sn doping on the structure is considered to be relatively strong. The strong suppression of the structural phase transition and promotion of the ferroelectric phase transition owing to Sn-substitution could be closely related to the ionic radius as well as the position of Sn within the structure. The Shannon–Prewitt ionic radii of 12-coordinated Sr^{2+} and Pb^{2+} are 1.44, and 1.49Å, respectively, [21] whereas that of Sn^{2+} is estimated to be 1.35 Å. [22] The large difference in the ionic radii together with the off-center position of Sn would tilt the oxygen octahedron from the crystal axes, resulting in the suppression of the structural phase transition, which is triggered by the freezing of the R_{25} mode associated with the collective antiphase rotation of the octahedral oxygen about the c-axis.

3.5 *Temperature dependence of the intensity of TO4 mode*

In a further step, the temperature dependence of the intensity of the TO4 mode, I_{TO4}, at ~555 cm^{-1} for SSTO x = 0.1 was investigated in the range of 120–510 K. To accurately measure the change in the intensity, the spectra are recorded at a point on the sample surface by monitoring the position using a

microscope. The beam-spot size is approximately 2 μm, which is larger than the average grain size. Figure 4 (a) shows the obtained Raman spectra. The values of I_{TO4} obtained by fitting to a damped harmonic oscillator (DHO) are plotted as a function of temperature in Figure 4(b). Upon cooling, I_{TO4} emerges at ~400 K and gradually increases. A rapid increase in I_{TO4} is observed for temperatures slightly higher than T_{m}. This behavior is similar to the temperature dependence of the polarization measured by Suzuki et al. and is shown in Figure 4(c). [6] Assuming that I_{TO4} in the paraelectric phase reflects the distribution of the local polarizations, this result suggests that local polar regions are expected to emerge below ~400 K and increase in volume as the temperature decreases. The discrepancy between the temperature dependence of I_{TO4} and that of the polarization shown in Figure 4(c) is attributed to the fact that Raman intensity is not associated with polarization but with electronic polarizability. Currently, the origin of such polar regions is not well-understood. Some explanations on this behavior would be possible, e.g., the effect of stress at the ceramic grain boundaries due to thermal expansion; percolation of local polarizations caused by the off-center position of the Sn atom; and the formation of polar nanoregions (PNRs), as observed in $Pb(Mn_{1/3}Nb_{2/3})O_3$ (PMN). [23] The Raman spectra in the low-frequency region, obtained at high temperatures using a powder sample, will aid the understanding of the origin of the polar regions and their influence on the ferroelectric phase transition and the peculiar dielectric responses observed. [24]

4 SUMMARY

Raman spectra were studied in the frequency range of 5–700 cm^{-1} in order to investigate the ferroelectric transition mechanism of $Sn_xSr_{1-x}TiO_3$ x = 0.02–0.1. Assuming that the symmetry of the ferroelectric phase in C_{4v}^1 symmetry as proposed by a recent neutron scattering study, the Raman peaks observed at ~26, 44, 77, and 120 cm^{-1} at 20 K were assigned to E (TO1), A_1 (TO1), E (LO1), and A_1 (LO1), respectively. The frequencies of the two TO1 modes decreased to considerably low frequencies in the region of their ferroelectric transition temperatures.

Raman spectra observed at higher temperatures revealed that polar local regions induced by the Sn atom emerge at ~400 K and grow as the temperature decreases. The increase in the spectral intensities around the zero frequency suggests the existence of a relaxation mode. Further analysis of the

spectra in the low-frequency region will lead to a thorough understanding of the influence of these polar regions on phase transitions and peculiar dielectric permittivity.

ACKNOWLEDGMENTS

Authors are grateful to Dr. S. Suzuki and Dr. A. Ando at Murata Manufacturing Co. Ltd. for providing us SSTO and PSTO samples and for stimulating discussions. T. N. thanks Assoc. Prof. T. Nezu at Health Science University of Hokkaido (HSUH) for his support in arranging experimental equipment. Parts of the experiments were performed at the High-Tech research center at HSUH.

REFERENCES

[1] V. V Lemanov, Phys. Solid State. **39** (1997) 1468–1473.

[2] V. V. Lemanov, Ferroelectrics. **226** (1999) 133–146.

[3] J.G. Bednorz, K.A. Muller, Phys. Rev. Lett. **52** (1984) 2289–2292.

[4] U. Bianchi, W. Kleemann, J.G. Bednorz, J. Phys. Condens. Matter. **6** (1994) 1229–1238.

[5] M. Itoh, R. Wang, Y. Inaguma, T. Yamaguchi, Y.J. Shan, T. Nakamura, Phys. Rev. Lett. **82** (1999) 3540–3543.

[6] S. Suzuki, A. Honda, N. Iwaji, S. Higai, A. Ando, H. Takagi, H. Kasatani, K. Deguchi, Phys.Rev.B**86** (2012) 060102(R).

[7] Y. Uratani, T. Shishidou, T. Oguchi, Jpn. J. Appl. Phys. **47** (2008) 7735–7739.

[8] S. Suzuki, A. Honda, K. Suzuki, S. Higai, A. Ando, K. Niwa, M. Hasegawa, Jpn. J. Appl. Phys. **52** (2013) 52–54.

[9] T. Nakano, Y. Mikami, K. Abe, S. Suzuki, K. Akiyama, A. Ando, Ferroelectrics. **464** (2014) 72–79.

[10] H. Kasatani, S. Suzuki, A. Ando, E. Magome, C. Moriyoshi, Y. Kuroiwa and K. Deguchi, Acta Cryst. (2014). A**70**, C61.

[11] G. Laurita, R. Seshadri, Phys. Rev. B**92** (2015)214109.

[12] G. Burns, B.A. Scott, Phys. Rev. B **7** (1973) 3088–3101.

[13] M. Jain, Y.I. Yuzyuk, R.S. Katiyar, Y. Somiya, A.S. Bhalla, J. Appl. Phys. **98** (2005) 24116.

[14] S. Suzuki, T. Takeda, A. Ando, H. Takagi, Appl. Phys. Lett. **96** (2010) 132903.

[15] H. Uwe, K. B. Lyons, H. L. Carter, and P. A. Fleury, Phys. Rev. B**33** (1986) 6436-6440.

[16] J. Frantti, V. Lantto, S. Nishio, and M. Kakihana, Phys. Rev. B**59** (1999) 12-15.

[17] S. M. Cho, J. H. Park, and H. M. Jang, J. Appl. Phys. **94** (2003) 1948-1953.

[18] J. Petzelt, T. Ostapchuk, I. Gregora, I. Rychetský, S. Hoffmann-Eifert, A. V Pronin, Y. Yuzyuk, B.P. Gorshunov, S. Kamba, V. Bovtun, J. Pokorný, M. Savinov, V. Porokhonskyy, D. Rafaja, P. Vaněk, A. Almeida, M.R. Chaves, A.A. Volkov, M. Dressel, R. Waser, Dielectric, Phys. Rev. B. **64** (2001) 184111.

[19] A.A. Sirenko, C. Bernhard, A. Golnik, A.M. Clark, J. Hao, W. Si, X.X. Xi, Nature. **404** (2000) 373–376.

[20] S. Banerjee, D. Kim, R.D. Robinson, I.P. Herman, Y. Mao, S.S. Wong, Appl. Phys. Lett. 89 (2006) 223130.

[21] R.D. Shannon, Acta Crystallogr. Sect. A. **32** (1976) 751–767.

[22] J.W. Bennett, I. Grinberg, P.K. Davies, A.M. Rappe, Phys. Rev. B. **83** (2011) 144112.

[23] G. Burns, B.A. Scott, Solid State Commun. **13** (1973) 423–426.

[24] J. Petzelt, S. Kamba, J. Hlinka, Ferroelectric soft modes in ceramics and films, chapter in the book *New*

developments in advanced functional ceramics 387-421(2007); arXiv:cond-mat/0611016.

Figure captions

Figure 1

(a) Raman spectra and (b) reduced Raman spectra $\mathrm{Im}\chi(\omega)$ of SSTO for x = 0.1, 0.05, and 0.02 in the frequency range of 5–80 cm^{-1}.

Figure 2

(a) Raman spectra of SSTO x = 0.1 in the frequency range of 15–700 cm^{-1} and (b) Raman spectra of PSTO x = 0.15 in the frequency range of 15–700 cm^{-1}. The inset is the spectra at 20 K in the range of 15–150 cm^{-1}. The shape of spectra below 20 cm^{-1} at 250 K for PSTO x=0.15 is artifact with the optical filter protecting CCD from the Rayleigh line.

Table 1

Mode assignment for SSTO x = 0.1 determined by referring to the Raman spectra of PSTO. The frequencies are approximate values, and all values are expressed in cm^{-1}.

Figure 3

Raman spectra of (a) SSTO x = 0.05 and (b) SSTO x = 0.02 in the frequency range of 15–700 cm^{-1}.

Figure 4

Raman spectra of SSTO x = 0.1 in the temperature range of 120–510 K. (b) Peak intensities of the TO4 mode as a function of temperature. Open circles represent the data measured using another experimental set-up. (c) The temperature dependence of the polarization of SSTO x = 0.1 reported by Suzuki et al. [6].

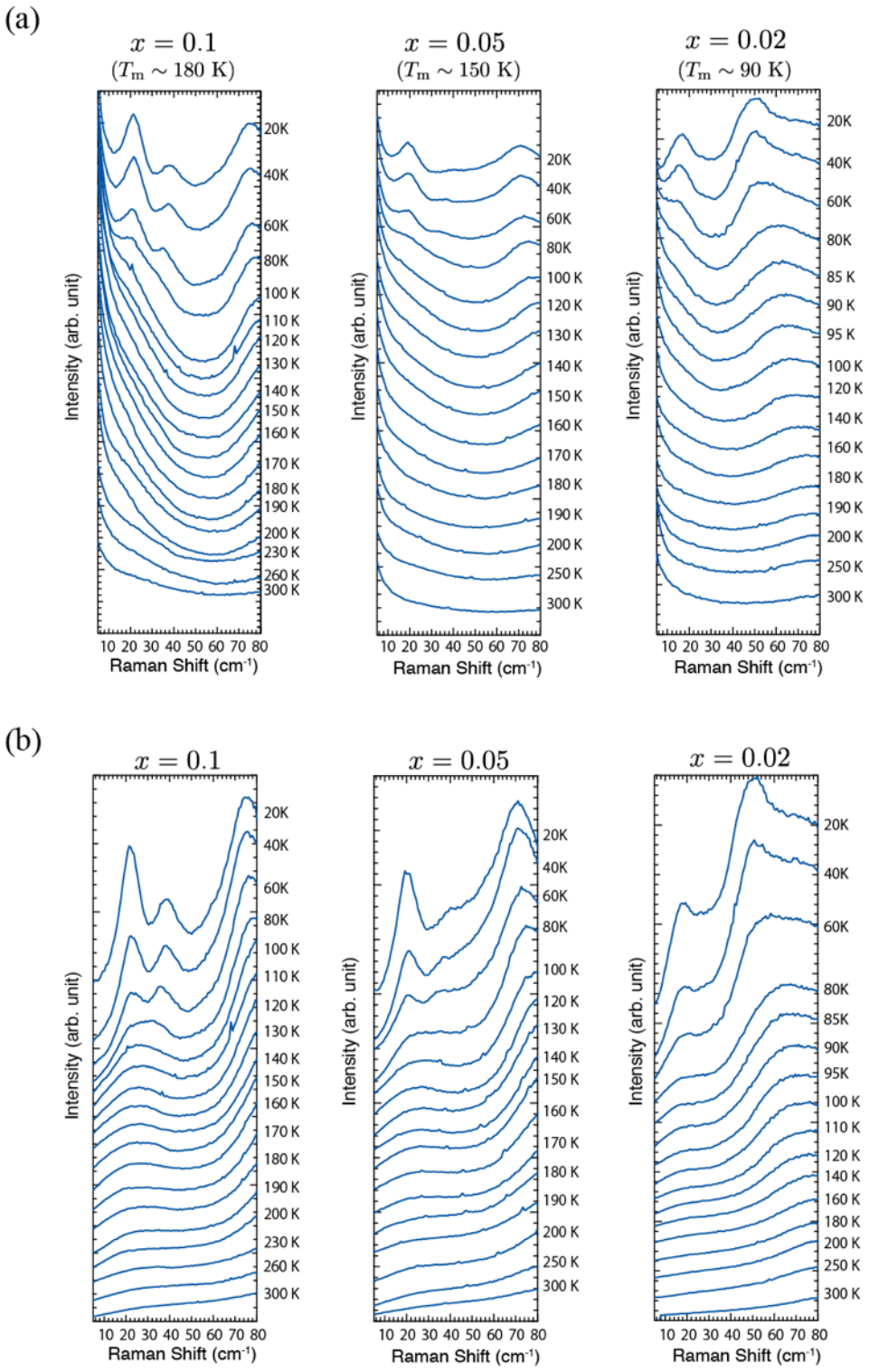
(a)
$x = 0.1$
($T_m \sim 180$ K)
$x = 0.05$
($T_m \sim 150$ K)
$x = 0.02$
($T_m \sim 90$ K)
Intensity (arb. unit)
Raman Shift (cm^{-1})
10 20 30 40 50 60 70 80
20K
40K
60K
80K
100 K
110 K
120 K
130 K
140 K
150 K
160 K
170 K
180 K
190 K
200 K
230 K
250 K
260 K
300 K
85 K
90 K
95 K
(b)
$x = 0.1$
$x = 0.05$
$x = 0.02$
85K
90K
95K

Figure 1

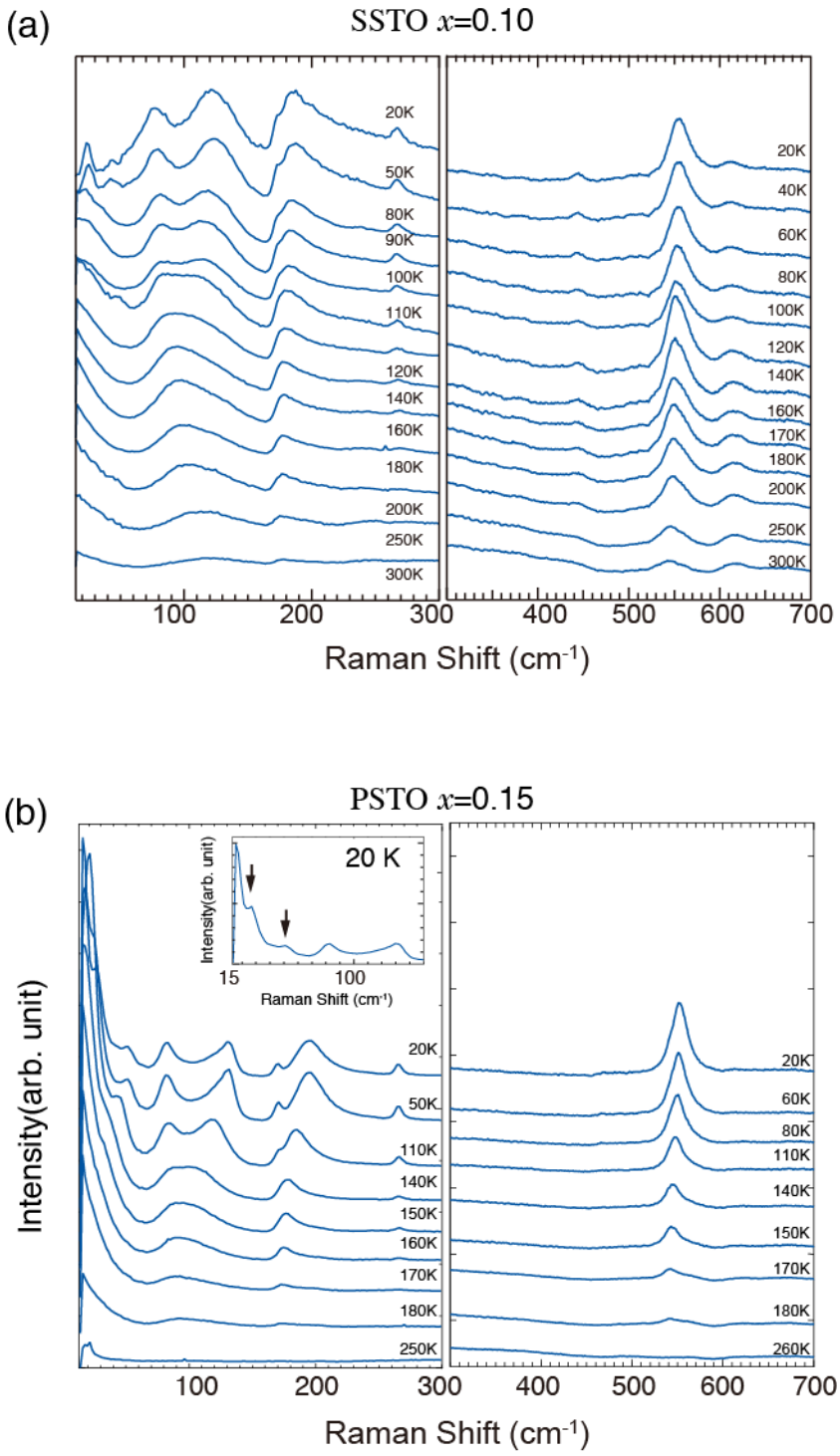
(a)
SSTO x=0.10
20K
50K
80K
90K
100K
110K
120K
140K
160K
180K
200K
250K
300K
20K
40K
60K
80K
100K
120K
140K
160K
170K
180K
200K
250K
300K
100
200
300
400
500
600
700
Raman Shift (cm^{-1})
(b)
PSTO x=0.15
20 K
Intensity(arb. unit)
15
100
Raman Shift (cm^{-1})
Intensity(arb. unit)
20K
50K
110K
140K
150K
160K
170K
180K
250K
20K
60K
80K
110K
140K
150K
170K
180K
260K
100
200
300
400
500
600
700
Raman Shift (cm^{-1})

Figure 2

SSTO $x = 0.1$

Paraelectric phase (300 K)		Ferroelectric phase (20 K)		
$Pm\bar{3}m$ (O_h^1)		$P4mm$ (C_{4v}^1)		
F_{1u}(TO1)	—	E	26	
		A_1	44	
F_{1u}(LO1)	~ 120	E	77	
		A_1	120	
F_{1u}(TO2)	~ 173	E	173	
		A_1	176	assymetric
F_{2u}(TO3)	—	$B_1 + E$	267	
F_{1u}(LO2)	—	$A_1 + E$	444	
F_{1u}(TO4)	545	E	555	

— not observed

Table 1

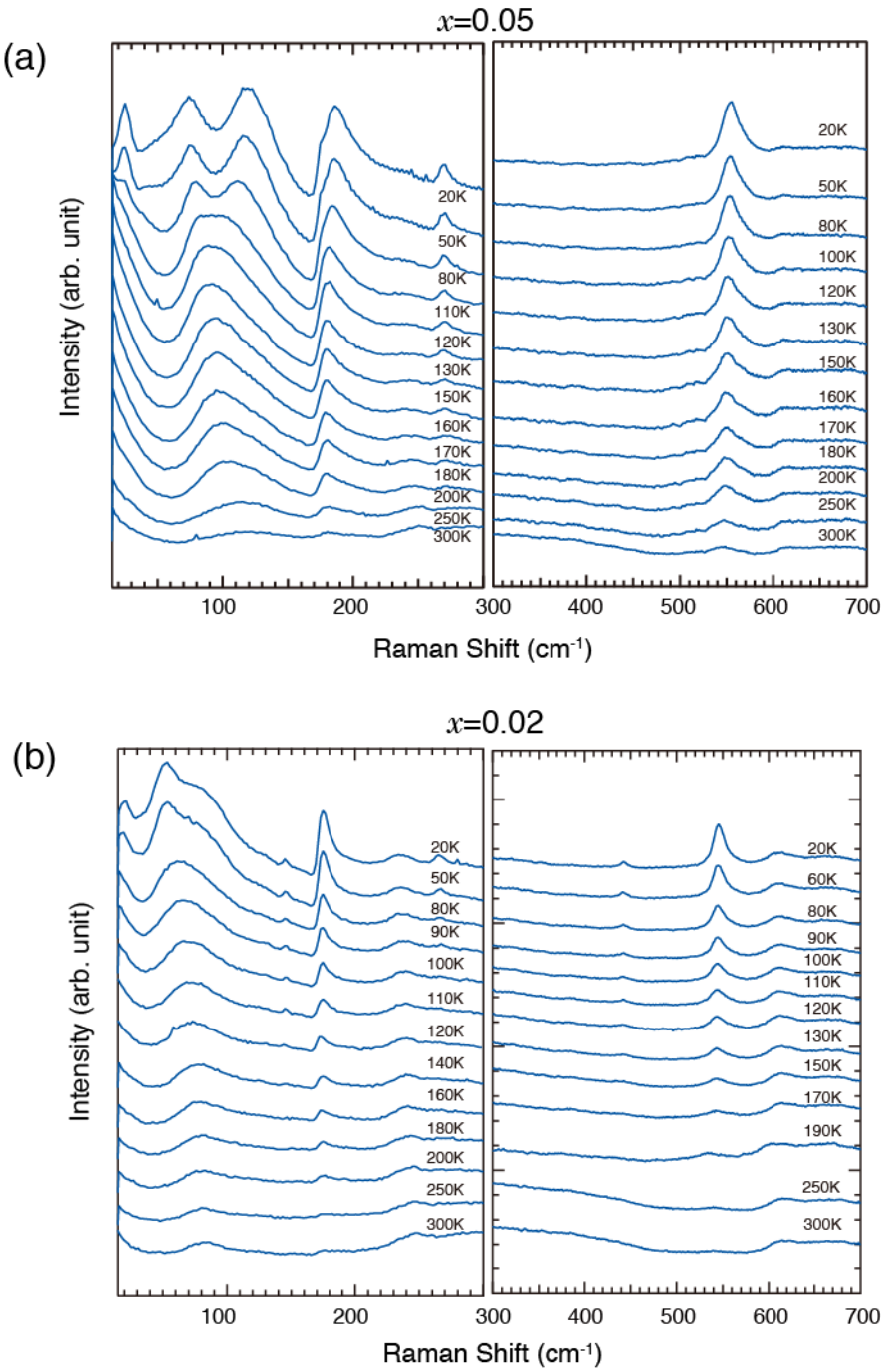
(a)
x=0.05
Intensity (arb. unit)
20K
50K
80K
110K
120K
130K
150K
160K
170K
180K
200K
250K
300K
100
200
300
400
500
600
700
Raman Shift (cm-1)
(b)
x=0.02
Intensity (arb. unit)
20K
50K
80K
90K
100K
110K
120K
140K
160K
180K
200K
250K
300K
60K
130K
150K
170K
190K
100
200
300
400
500
600
700
Raman Shift (cm-1)

Figure 3

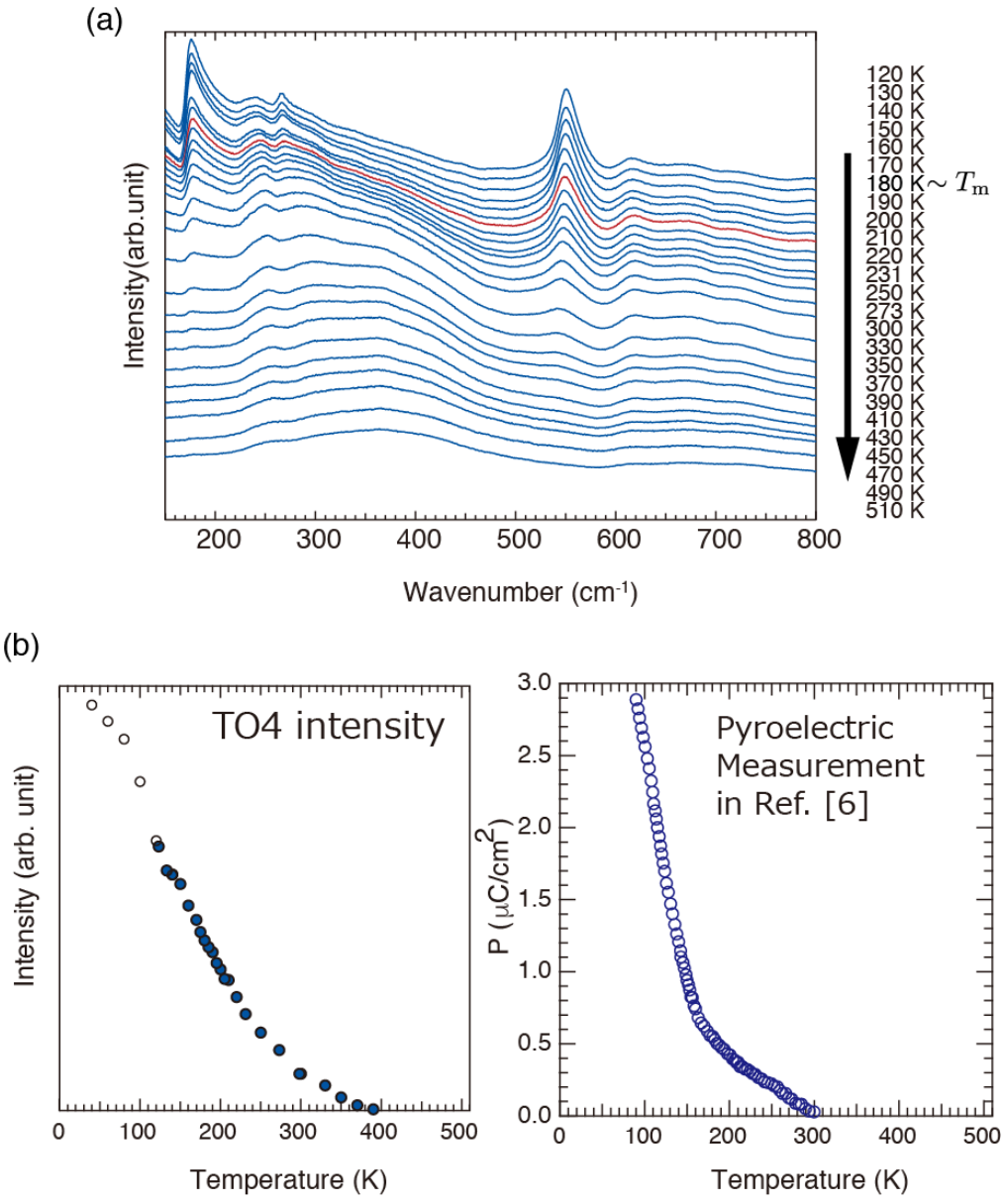
(a)
Intensity(arb.unit)
Wavenumber (cm-1)
120 K
130 K
140 K
150 K
160 K
170 K
180 K
190 K
200 K
210 K
220 K
231 K
250 K
273 K
300 K
330 K
350 K
370 K
390 K
410 K
430 K
450 K
470 K
490 K
510 K
~ Tm
(b)
TO4 intensity
Intensity (arb. unit)
Temperature (K)
Pyroelectric
Measurement
in Ref. [6]
P (μC/cm2)
Temperature (K)

Figure 4